The Magnetic Signatures of the M_2, N_2, and O_1 Oceanic Tides Observed in Swarm and CHAMP Satellite Magnetic Data

Grayver, Alexander V.; Olsen, Nils

Published in:
Geophysical Research Letters

Link to article, DOI:
10.1029/2019GL082400

Publication date:
2019

Document Version
Publisher's PDF, also known as Version of record

Geophysical Research Letters

RESEARCH LETTER
10.1029/2019GL082400

The Magnetic Signatures of the M_2, N_2, and O_1 Oceanic Tides Observed in Swarm and CHAMP Satellite Magnetic Data

Alexander V. Grayver[1] **and Nils Olsen**[2]

[1]Institute of Geophysics, ETH Zürich, Zürich, Switzerland, [2]DTU Space, Technical University of Denmark, Kongens Lyngby, Denmark

Key Points:
- Global models of the magnetic signals produced by the M_2, N_2, and O_1 oceanic tides have been extracted from satellite magnetic measurements
- Combining data from the Swarm and CHAMP missions as well as using field gradient plays key role in the robustness of the estimated models
- All tidal constituents show significant sensitivity to the electrical conductivity of the oceanic mantle

Supporting Information:
- Supporting Information S1
- Movie S1
- Movie S2
- Movie S3
- Data Set S4
- Data Set S5
- Data Set S6

Correspondence to:
A. V. Grayver,
agrayver@erdw.ethz.ch

Citation:
Grayver, A. V., & Olsen, N. (2019). The magnetic signatures of the M_2, N_2, and O_1 oceanic tides observed in Swarm and CHAMP satellite magnetic data. *Geophysical Research Letters*, *46*. https://doi.org/10.1029/2019GL082400

Received 8 FEB 2019
Accepted 8 APR 2019
Accepted article online 15 APR 2019

Abstract This paper reports on new results in the determination of magnetic signals produced by oceanic tides as estimated from satellite magnetic measurements. We find that combining data from the past CHAMP (2000–2010) and the present Swarm (since 2013) satellite missions significantly improves the quality of the extracted tidal signals, in particular if along-track and cross-track magnetic "gradient" data are utilized. This allows us to determine the magnetic signature not only of the M_2 tide but also of the much weaker N_2 and O_1 tidal constituents. To minimize disturbances from magnetospheric and ionospheric currents, we only use data from the nightside region during geomagnetic quiet conditions and remove core, crustal, and magnetospheric field contributions as given by the CHAOS geomagnetic field model. Despite their small magnitudes, all determined tidal constituents show sensitivity to the electrical conductivity profile of the underlying mantle, enabling imaging the upper mantle below the oceans.

1. Introduction

Tidal motion of the electrically conducting seawater in the oceans produces a magnetic field signature by means of a phenomena called motional induction (Chave & Luther, 1990; Sanford, 1971; Tyler et al., 1997). The first successful attempt to globally determine the weak magnetic tidal signal (of the strongest lunar tidal constituent, M_2) used 2 years of magnetic observations taken by the CHAMP satellite mission (Tyler et al., 2003). This work demonstrated the remarkable high quality of satellite magnetic data and envisaged some applications of the determined M_2 signal, although these applications were hindered by insufficient quality of the magnetic tidal determination at that time. This has changed with the release of the "Comprehensive Model 5" (CM5) (Sabaka et al., 2015), which, among others, resulted in a substantially improved quality of the extracted M_2 magnetic tidal signal, enabling its use for probing the electrical conductivity of the upper mantle beneath the oceans (Grayver et al., 2016; Schnepf et al., 2015). These papers demonstrated feasibility of using satellite-detected magnetic tidal signals as an electromagnetic induction source for imaging the upper mantle below the oceans on a global scale, complementing previous attempts based on local measurements of tidal electromagnetic (EM) signals for conductivity sounding (e.g., Larsen, 1968; Kuvshinov et al., 2006). This source aims at complementing marine magnetotellurics (e.g., Evans et al., 2005; Naif et al., 2013), an alternative method to study oceanic upper mantle but with coverage limitations due to its high cost and inherent logistical challenges. Therefore, a successful determination of tidal constituents other than the dominant M_2 mode, and improving overall signal quality, will lead to better constrained electrical structure of the oceanic mantle. Furthermore, other applications such as remote sensing of the ocean dynamics will benefit from improved models of tidal magnetic signals (e.g., Minami, 2017; Saynisch et al., 2017; Trossman & Tyler, 2019).

The CM5 magnetic field model is based on magnetic data taken by the pre-Swarm satellite missions Ørsted, CHAMP, and SAC-C. Although these missions all consist of a single satellite, the data set includes a particularly favorable period between 2007 and 2010 when CHAMP was flying at low altitudes during a solar minimum. In contrast, the three-satellite constellation mission Swarm (in operation since November 2013) enables measuring the East-West (mainly cross-track) magnetic field gradient (approximated in practice by finite differences of simultaneous observations taken by the side-by-side flying satellites Swarm Alpha and Charlie), in addition to the along-track gradient (approximated by finite differences of succeeding measurements taken by a single satellite). This results in an improved determination of the M_2 signal (Sabaka et al.,

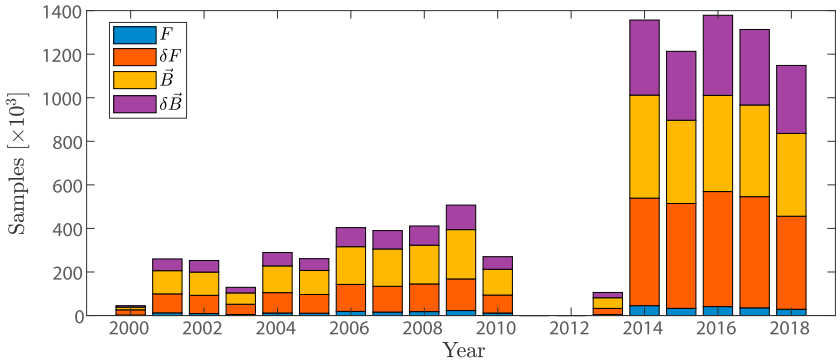

Figure 1. Time distribution of the satellite data used in this study. Period prior to 2011 corresponds to the CHAMP satellite data while period after 2013 to the Swarm phase. Symbols $F, \delta F, \vec{B},$ and $\delta\vec{B}$ denote scalar, scalar difference, vector, and vector difference data, respectively.

2016, 2018) despite the higher solar activity and altitude as compared to CHAMP. So far, the combined analysis of both CHAMP and Swarm data for tidal signals has not been reported. Furthermore, most studies used the "Comprehensive Inversion" approach, which strives for a consistent coestimation of various magnetic field sources by accounting for various dependencies and correlations of the data and modeled sources. However, the comprehensive inversion approach is very resource and time demanding and thus suboptimal for hypothesis testing and optimal parameter search. A sequential approach, focusing on determination of tidal signals from magnetic field residuals (i.e., observations minus model predictions of nontidal fields like core and crustal field contributions) is much faster and thus better suited for parameter optimization experiments.

Global determination of tidal constituents other than M_2 is challenging due to the much smaller amplitudes, although some promising results have been obtained in regions where the signals are strong (e.g., Maus & Kuvshinov, 2004; Sabaka et al., 2016). Constituents other than M_2 would provide additional constraints on the mantle conductivity in regions where M_2 is weak. Further, even though some constituents may have very similar periods (for instance, M_2 and N_2), their flows and hence generated electric currents differ, thus leading to unique sensitivity footprints. The latter property may be particularly advantageous for exploring lateral conductivity heterogeneities in the mantle.

Motivated by these arguments, current study aims at extracting magnetic signatures of the three tidal constituents M_2, N_2, and O_1 by joint analysis of CHAMP and Swarm satellite magnetic data. Because of its simplicity and speed, we adopt the sequential approach which enables a systematic testing of various model parametrizations and data selection criteria.

2. Methodology

2.1. Data Selection

The analysis is based on magnetic field observations taken by the CHAMP and Swarm satellites. CHAMP data between 2000 and 2010 and Swarm data between November 2013 and September 2018 were used. We do not include any ground magnetic observatory data and rely solely on satellite measurements. The data selection criteria are identical to those used for deriving the CHAOS-6 model (Finlay et al., 2016) with the only exception that we exclude any dayside data and thus only work with data from the dark side (sun at least 10° below the horizon). This is done to minimize the effects of the lunar ionospheric tidal signals, which contaminate oceanic signals on the day side (e.g., Alken & Maus, 2007; Malin & Chapman, 1970; Olsen, 1997; Schnepf et al., 2018). Both vector and scalar fields and their along- and cross-track differences are used (see Finlay et al., 2016, for details), resulting in $3 \times 1,174,834$ vector data, $3 \times 799,337$ vector differences, 326,417 scalar data, and 1,534,374 scalar differences distributed in time as shown in Figure 1. Following Finlay et al. (2016), we use scalar data only poleward of the ±55° quasi-dipole latitude, resulting in a relatively small amount of scalar field observations.

To account for the core, lithosphere, and large-scale magnetospheric components, we subtract from the

Table 1
Tidal Constituents, Their Period T, and Maximum Spherical Harmonic Degree N_{max} Used in the Model Parametrization

Constituent	T (hr)	$N_{\max}$
M_2	12.4206	28
N_2	12.6583	12
O_1	25.8193	12

observations model predictions of these three sources as given by the CHAOS-6 model (version x7). The obtained residuals comprise the input data for this study.

2.2. Signal Extraction

Our model parametrization follows Sabaka et al. (2018): The magnetic signal $\vec{B} = -\nabla V(t, \vec{r})$ of tides is represented by a magnetic scalar potential V. At time t and position $\vec{r}$, V is expanded via spherical harmonics as

$$V(t,\vec{r}) = \mathrm{Re}\left\{ \exp(i\omega t) R_E \sum_{n=1}^{N_{\max}} \left(\frac{R_E}{r}\right)^{n+1} \sum_{m=-n}^{n} \tau_n^m P_n^{|m|}(\cos\theta) \exp(im\phi) \right\}, \quad (1)$$

where $R_E = 6,371.2$ km is Earth's mean radius; $\vec{r} = (r, \theta, \phi)$ is the position vector with ϕ, θ being geographic longitude and colatitude, respectively; τ_n^m are complex spherical harmonic coefficients of spherical harmonic degree n and order m; $P_n^{|m|}$ are Schmidt semi-normalized associated Legendre functions; angular frequencies $\omega = 2\pi/T$ with T being the period of a tidal constituent; and Re$(\cdot)$ denotes the real part. Different tidal constituents are estimated separately using the period T and maximum spherical harmonic degree $N_{\max}$ as listed in Table 1. $N_{\max}$ is chosen based on numerous trials as a trade-off between low noise levels and high spatial resolution. More data in the future will likely enable higher resolution of the extracted signals without compromising their quality.

We use robust linear regression (iteratively reweighted least squares,; Aster et al., 2018; with Huber weights, Constable, 1988) to estimate the spherical harmonic coefficients τ_n^m for each of the three tidal constituents. This robust approach is similar to the one described, for example, in Olsen et al. (2017) with some modifications explained in Supporting Information S1.

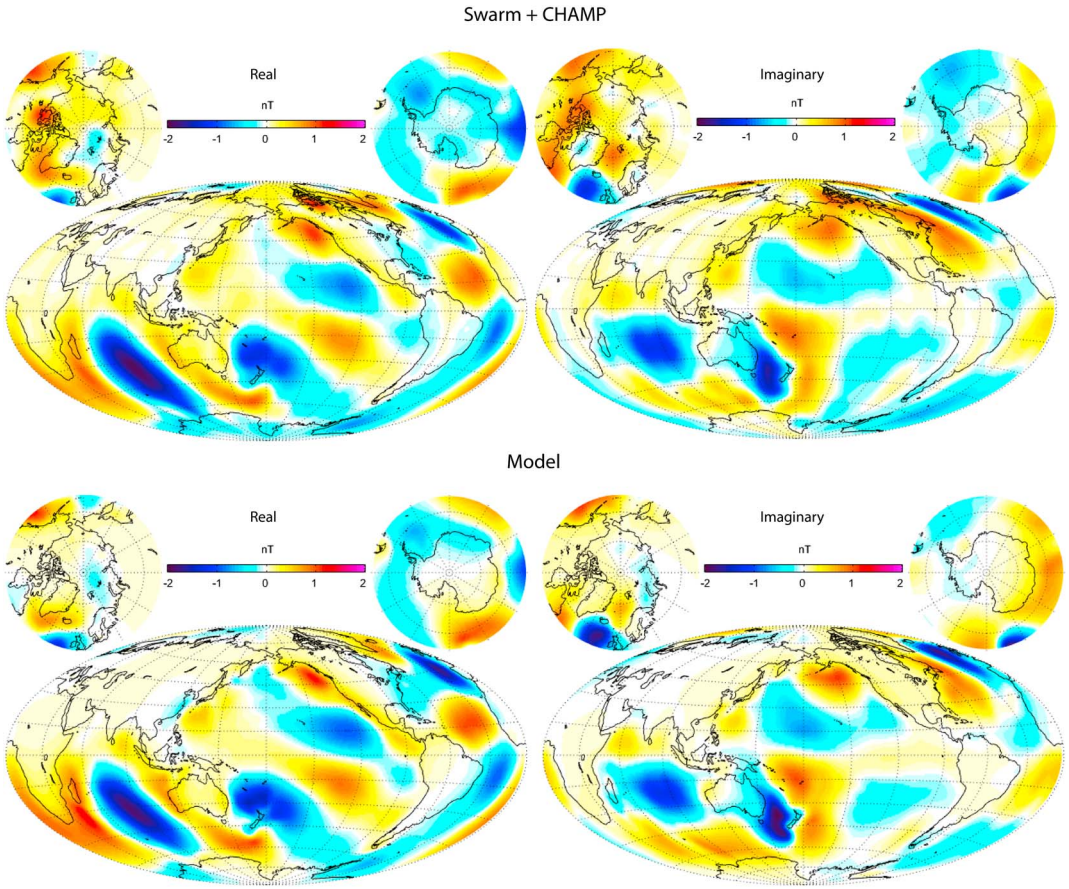

Figure 2. Estimated (top) and simulated (bottom) magnetic radial component due to the M_2 tide. Shown are real (left) and imaginary (right) parts of the signal at 430-km altitude.

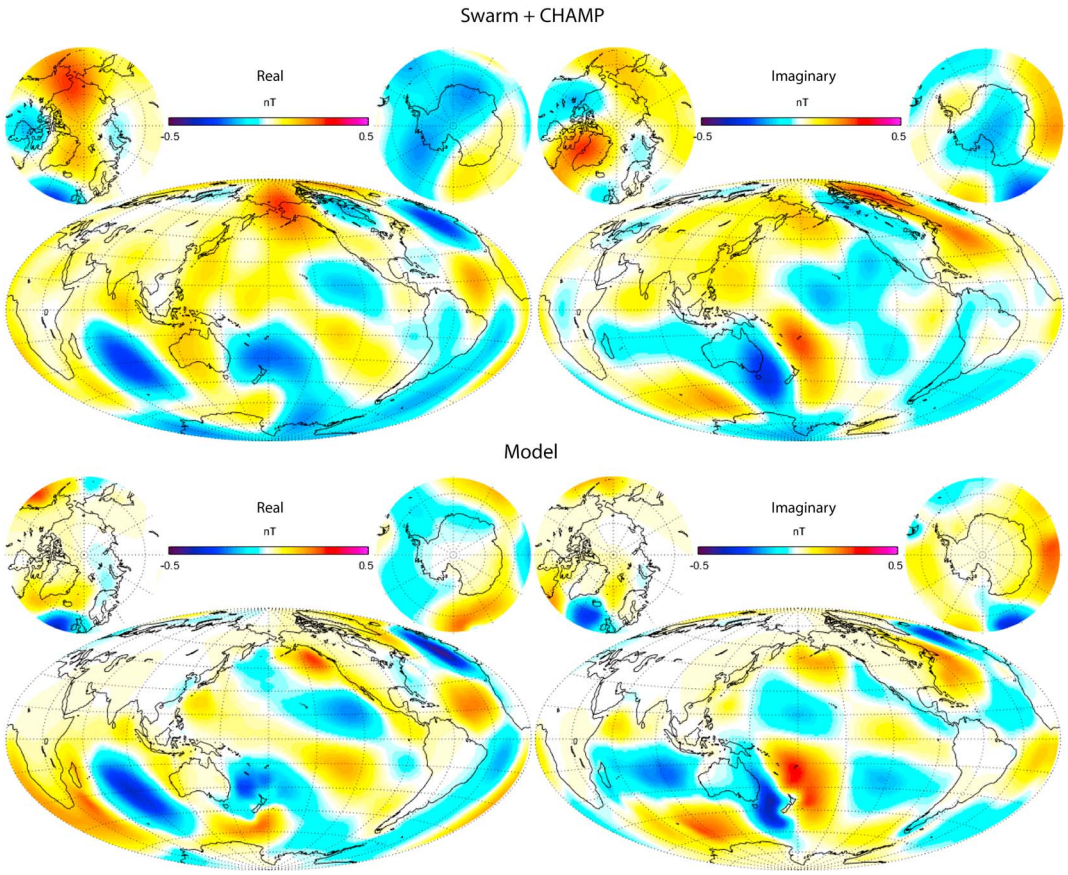

Figure 3. Same as Figure 2 but for the N_2 tide.

Following previous studies, the spatial power spectrum at altitude corresponding to radius r is defined as

$$R_n(r) = \frac{n+1}{2}\left(\frac{R_E}{r}\right)^{2n+4}\left[|\tau_n^0|^2 + \sum_{m=1}^{n}\left(|\tau_n^m|^2 + |\tau_n^{-m}|^2\right)\right]. \quad (2)$$

2.3. Forward Modeling of Tidal Magnetic Signals

In order to compare the estimated tidal signals with theoretical values, we performed numerical simulations using the radial mantle conductivity profile of Grayver et al. (2017) overlaid by a shell with heterogeneous conductivities representing the ocean and sediments (Manoj et al., 2006). The electrical current source $\mathbf{u} \times \mathbf{B}_0$ is given by the TPXO9 model (Egbert & Erofeeva, 2002) of tidal transport $\mathbf{u}$ and the IGRF-12 magnetic field model (Thébault et al., 2015) for the ambient magnetic field $\mathbf{B}_0$. We solve the full Maxwell's equations using a finite-element global electromagnetic solver (Grayver et al., 2019) that is based on several open-source libraries (Alzetta et al., 2018; Balay et al., 2018; Karypis & Kumar, 1999) In simulations, the ocean is galvanically coupled to the mantle, resulting in a bimodal-induced fields (Chave & Luther, 1990; Velímsky et al., 2018). In the study case of an insulating mantle, a conductivity of 10^{-7} S/m is formally assigned.

3. Results

Figures 2 to 4 compare observed (top) and modeled (bottom) radial magnetic field components for each of the three tidal constituents analyzed in this study. The dominant M_2 tide (Figure 2) produces magnetic signals up to 2 nT at 430-km altitude and reveals, similar to previous studies, an observed signals (top) that is in remarkably good agreement with the simulated fields (bottom). However, the fascinating and novel outcome of this study is that we additionally determined globally the much weaker N_2 (Figure 3) and O_1 (Figure 4) magnetic signals. The amplitudes of these signals hardly reach 0.5 nT at satellite altitudes, yet the agreement with the simulation results is very good, particularly at middle and low latitudes. The larger

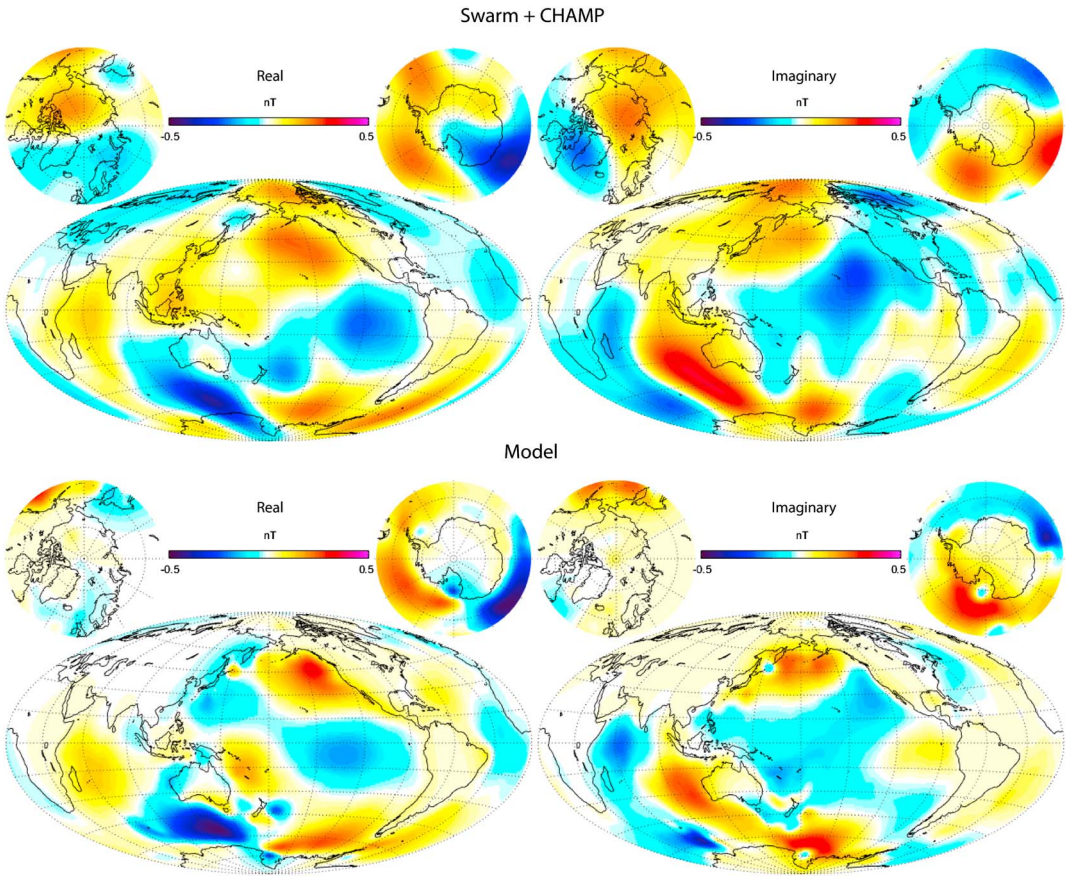

Figure 4. Same as Figure 2 but for the O_1 tide.

discrepancy at polar latitudes originates likely from contamination by ionospheric polar currents, which we do not account for in this study. Nevertheless, the contaminant signals are on the order of $0.1 - 0.2$ nT and remain acceptable.

Spatial power spectra R_n (equation (2)) of the observed magnetic tidal fields are shown in Figure 5. For reference, we also show spectra of the simulated signals for an insulating, respectively electrically conductive, mantle. Their difference demonstrates that all tidal constituents, including the weaker N_2 and O_1 constituents, exhibit sensitivity to the electrical conductivity of the underlying mantle: The spectra of the observed field follow more closely those of the simulated signals for a conducting mantle. An insulating mantle produces much stronger magnetic signals due to the absence of attenuation in the mantle. Despite this model likely does not represent reality, it gives an upper bound on the noise level, hence providing an objective criterion for evaluating the quality of the extracted signal. For instance, the low-degree ($n = 1 - 3$) part of the O_1 spectrum, where the observations are higher than the insulating mantle spectrum, might be contaminated by fields of magnetospheric origin and thus should be interpreted with care.

In order to study the key aspects which enable the extraction of the weak N_2 and O_1 tidal signals, we now investigate the effect of combining CHAMP and Swarm satellite data, as well as the role of field difference ("gradient") data. Figure 6 (top row) shows spatial spectra for signals obtained by analyzing CHAMP, respectively Swarm, data separately and jointly. Clearly, combining data from both satellite missions significantly improves the signal-to-noise ratio and stabilizes the obtained solution. Further, Figure 6 (bottom row) shows the effect of using different data types. It is clear that excluding field difference (gradient) data and working only with field data leads to less reliable solutions, especially for spherical harmonic degrees $n > 5$, where gradients likely help suppress contamination by unmodeled (probably ionospheric and magnetospheric) contributions. On the other hand, excluding field data and relying only on the field differences results in a very unstable model. This finding is different from the experience in lithospheric modeling (e.g., Kotsiaros et al., 2014; Olsen et al., 2017) where very good results were obtained from an analysis of gradi-

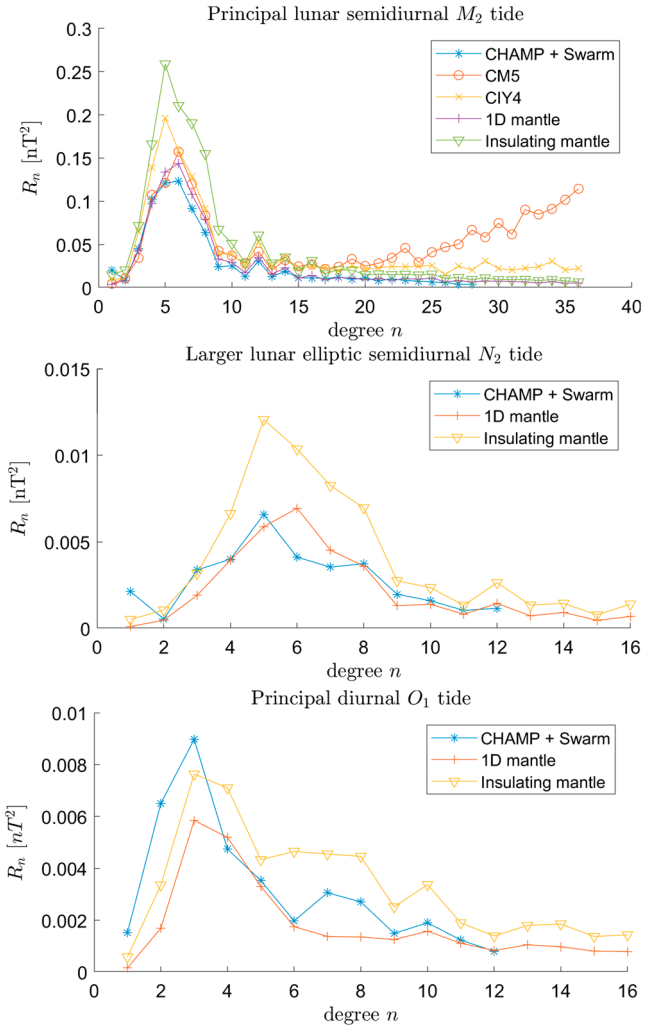

Figure 5. Spatial power spectra R_n of the extracted and simulated tidal signals at Earth's surface. (top) M_2 spectra from this study (denoted as "CHAMP + Swarm") and spectra obtained in previous studies (CM5 denotes "Comprehensive Model 5," Sabaka et al., 2015; and CIY4 denotes "Comprehensive Inversion Year 4," Sabaka et al., 2018). For reference, spectra of the simulated fields based on a 1-D conductivity profile and an insulating mantle are given (see section 2.3). (middle and bottom) Same as top but for the N_2 and O_1 tidal constituents, respectively.

ent data alone, probably due to the smaller spatial scale of the lithospheric field which favorites gradient information. In contrast, for the determination of the magnetic signature of oceanic tides, the gradient data play an important role, but the inclusion of field data remains crucial.

Animations of the time dependence of the tidal signals for all constituents are given in Supporting Information S1.

3.1. Implications for Conductivity of Oceanic Mantle

We tested the sensitivity of both the new and previously extracted signals to the conductivity values of the lithosphere and astenosphere by means of a two-parameter model. Assuming an average oceanic lithosphere thickness of 70 km (Rychert & Shearer, 2009), we varied the conductivity values of the two layers and calculated the root-mean-square (RMS) error between the calculated and observed radial magnetic field components at satellite altitude (430 km). We used tidal signals obtained in this study and the M_2 signal from the CM5 model (Sabaka et al., 2015). Errors derived from the formal posterior covariance matrix (Aster et al., 2018) were used to normalize the misfit. Figures 7a and 7b show the RMS as a function of the lithosphere and astenosphere conductivity. Although the absolute RMS error depends on the data uncertainty, the slopes and location of the minimum in the plots characterize the sensitivity and the most probable solution, respectively. Figures 7c and 7d show centered RMS profiles for the best fit parameters. First of all, one sees a good

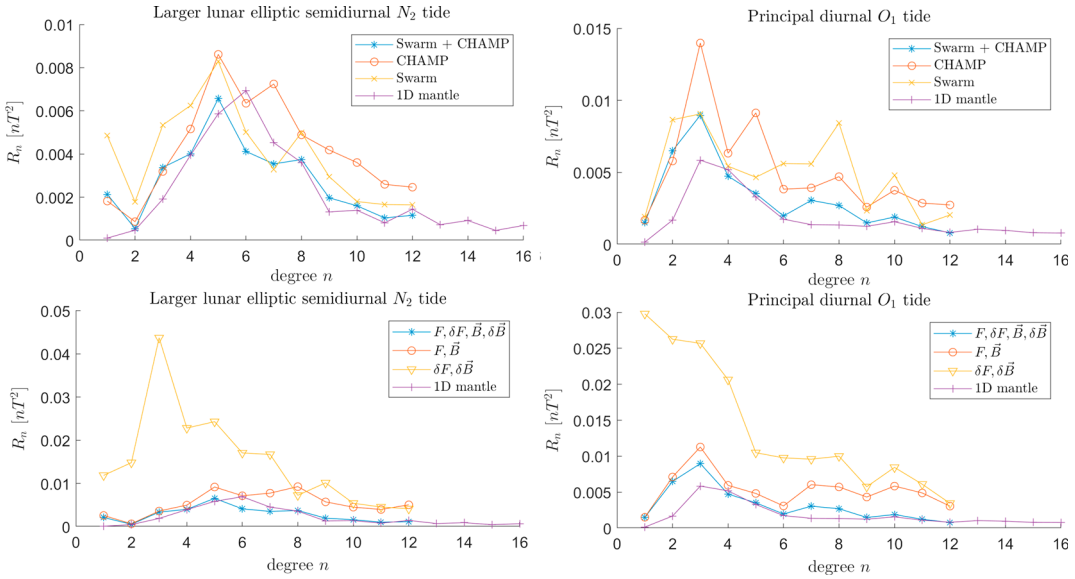

Figure 6. Spatial power spectra of the N_2 and O_1 signals at Earth's surface. (top row) Signals estimated from either CHAMP or Swarm data as well as using data from both missions. (bottom row) Signals estimated using either field data or field difference ("gradient") data, as well as using both of them. For reference, spectra of the modeled fields using a 1-D mantle conductivity profile are given.

agreement between the most probable solutions from CM5 and present study signals, which shows the high quality of CM5, but also confirms that the approach adopted here provides reliable estimates. The current tidal signals suggest a slightly more conductive astenosphere and a more resistive lithosphere. While this is favored by laboratory conductivity profiles (Grayver et al., 2017), the differences may lie within the uncertainty and should be confirmed with future additional data. Additionally, steep slopes for the present signals indicate higher sensitivity to the conductivity variations in the mantle.

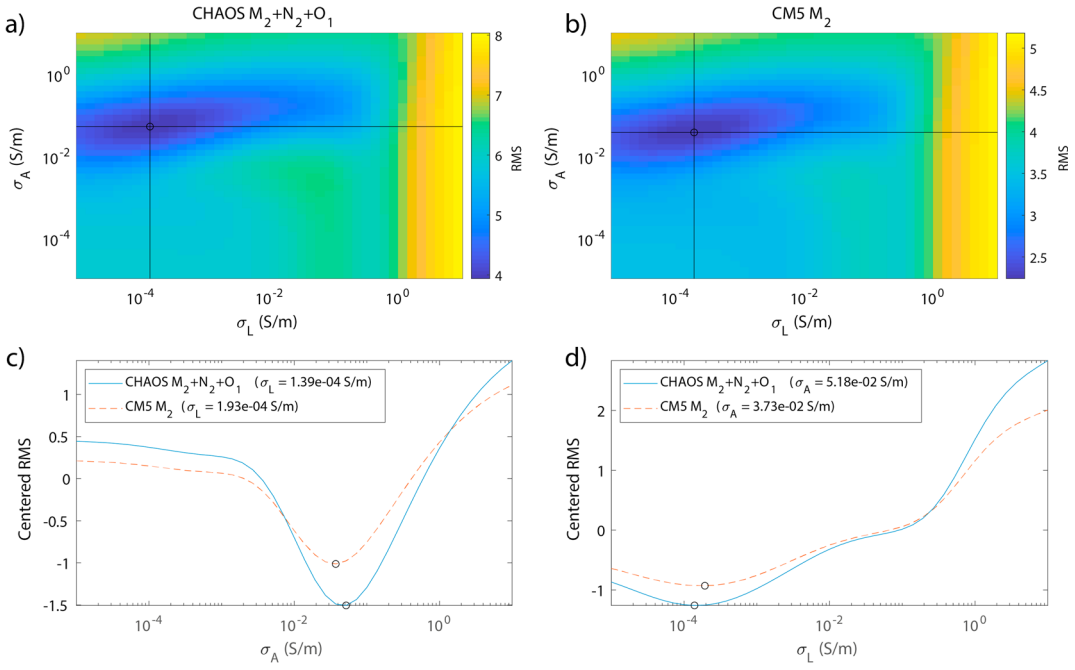

Figure 7. (a, b) RMS error between simulated and observed signals for various conductivity values of the astenosphere (σ_A) and a 70-km-thick lithosphere (σ_L). Black circles indicate the position of the minimum. (c, d) Graphs of the centered RMS values along black lines shown in (a) and (b). Legend items show conductivity values of the corresponding conditional variable. CM5 = Comprehensive Model 5; RMS = root-mean-square.

4. Conclusions

We provide the first global observation of the magnetic signatures generated by the N_2 and O_1 oceanic tides, based on a combined analysis of 10 years of CHAMP and almost 5 years of Swarm satellite magnetic data. Along-track and cross-track field difference (gradient) data play a key role in obtaining robust estimates at smaller spatial scales. Additional forthcoming data from Swarm may potentially make an extraction of even weaker tidal constituents feasible. As we enter a period of low solar activity and the Swarm satellite altitude naturally descend, new data are likely to further increase the quality of the obtained models, hence refining our knowledge about oceanic mantle.

Acknowledgments
We thank ESA for rapid and easy access to the Swarm Level 1b data, which are available from ESA (http://earth.esa.int/swarm). The support of the CHAMP mission by the German Aerospace Center (DLR) and the Federal Ministry of Education and Research is gratefully acknowledged. This work was supported by ESA through the Swarm DISC project. Spherical harmonic expansion coefficients of the estimated tidal signals are available in the supporting information. We thank Alexey Kuvshinov, Chris Finlay, and Lars Tøffner-Clausen for insightful discussions on the data processing and modeling. Comments by Richard Holme and Jakub Velimsky helped improve the quality of the paper.

References

Alken, P., & Maus, S. (2007). Spatio-temporal characterization of the equatorial electrojet from CHAMP, Ørsted, and SAC-C satellite magnetic measurements. *Journal of Geophysical Research*, *112*, A09305. https://doi.org/10.1029/2007JA012524

Alzetta, G., Arndt, D., Bangerth, W., Boddu, V., Brands, B., Davydov, D., et al. (2018). The deal. ii library, version 9.0. *Journal of Numerical Mathematics*, *26*(4), 173–183.

Aster, R. C., Borchers, B., & Thurber, C. H. (2018). *Parameter estimation and inverse problems*. Amsterdam, Netherlands: Elsevier.

Balay, S., Abhyankar, S., Adams, M. F., Brown, J., Brune, P., Buschelman, K., et al. (2018). PETSc users manual (ANL-95/11 - Revision 3.10). Lemont, IL: Argonne National Laboratory.

Chave, A. D., & Luther, D. S. (1990). Low-frequency, motionally induced electromagnetic fields in the ocean. 1. Theory. *Journal of Geophysical Research*, *95*, 7185–7200.

Constable, C. (1988). Parameter estimation in non-Gaussian noise. *Geophysical Journal*, *94*(1), 131–142.

Egbert, G. D., & Erofeeva, S. Y. (2002). Efficient inverse modeling of barotropic ocean tides. *Journal of Atmospheric and Oceanic Technology*, *19*(2), 183–204.

Evans, R. L., Hirth, G., Baba, K., Forsyth, D., Chave, A., & Mackie, R. (2005). Geophysical evidence from the MELT area for compositional controls on oceanic plates. *Nature*, *437*(7056), 249–252.

Finlay, C. C., Olsen, N., Kotsiaros, S., Gillet, N., & Tøffner-Clausen, L. (2016). Recent geomagnetic secular variation from Swarm and ground observatories as estimated in the CHAOS-6 geomagnetic field model. *Earth, Planets and Space*, *68*(1), 112.

Grayver, A. V., Munch, F. D., Kuvshinov, A. V., Khan, A., Sabaka, T. J., & Tøffner-Clausen, L. (2017). Joint inversion of satellite-detected tidal and magnetospheric signals constrains electrical conductivity and water content of the upper mantle and transition zone. *Geophysical research letters*, *44*, 6074–6081. https://doi.org/10.1002/2017GL073446

Grayver, A. V., Schnepf, N. R., Kuvshinov, A. V., Sabaka, T. J., Manoj, C., & Olsen, N. (2016). Satellite tidal magnetic signals constrain oceanic lithosphere-asthenosphere boundary. *Science Advances*, *2*(9), e1600798.

Grayver, A. V., van Driel, M., & Kuvshinov, A. V. (2019). Three-dimensional magnetotelluric modeling in spherical Earth. *Geophysical Journal International*, *217*, 532–557.

Karypis, G., & Kumar, V. (1999). A fast and highly quality multilevel scheme for partitioning irregular graphs. *Journal on Scientific Computing*, *20*(1), 359–392.

Kotsiaros, S., Finlay, C., & Olsen, N. (2014). Use of along-track magnetic field differences in lithospheric field modelling. *Geophysical Journal International*, *200*(2), 880–889.

Kuvshinov, A., Junge, A., & Utada, H. (2006). 3-D modelling the electric field due to ocean tidal flow and comparison with observations. *Geophysical Research Letters*, *33*, L06314. https://doi.org/10.1029/2005GL025043

Larsen, J. (1968). Electric and magnetic fields induced by deep sea tides. *Geophysical Journal of the Royal Astronomical Society*, *16*(1), 47–70.

Malin, S., & Chapman, S. (1970). Lunar tidal components N_2 and O_1 in the atmospheric pressure. *Pure and Applied Geophysics*, *80*(1), 309–318.

Manoj, C., Kuvshinov, A., Maus, S., & Lühr, H. (2006). Ocean circulation generated magnetic signals. *Earth, Planets and Space*, *58*(4), 429–437.

Maus, S., & Kuvshinov, A. (2004). Ocean tidal signals in observatory and satellite magnetic measurements. *Geophysical Research Letters*, *31*, L15313. https://doi.org/10.1029/2004GL020090

Minami, T. (2017). Motional induction by tsunamis and ocean tides: 10 years of progress. *Surveys in Geophysics*, *38*(5), 1097–1132.

Naif, S., Key, K., Constable, S., & Evans, R. (2013). Melt-rich channel observed at the lithosphere-asthenosphere boundary. *Nature*, *495*(7441), 356–359.

Olsen, N. (1997). Geomagnetic tides and related phenomena. In *Tidal phenomena* (pp. 261–274). Berlin, Heidelberg: Springer.

Olsen, N., Ravat, D., Finlay, C. C., & Kother, L. K. (2017). LCS-1: A high-resolution global model of the lithospheric magnetic field derived from CHAMP and Swarm satellite observations. *Geophysical Journal International*, *211*(3), 1461–1477.

Rychert, C. A., & Shearer, P. M. (2009). A global view of the lithosphere-asthenosphere boundary. *Science*, *324*(5926), 495–498.

Sabaka, T. J., Olsen, N., Tyler, R. H., & Kuvshinov, A. (2015). CM5, a pre-Swarm comprehensive geomagnetic field model derived from over 12 yr of CHAMP, Ørsted, SAC-C and observatory data. *Geophysical Journal International*, *200*(3), 1596–1626.

Sabaka, T. J., Tøffner-Clausen, L., Olsen, N., & Finlay, C. C. (2018). A comprehensive model of Earth's magnetic field determined from 4 years of swarm satellite observations. *Earth, Planets and Space*, *70*(1), 130.

Sabaka, T. J., Tyler, R. H., & Olsen, N. (2016). Extracting ocean-generated tidal magnetic signals from Swarm data through satellite gradiometry. *Geophysical Research Letters*, *43*, 3237–3245. https://doi.org/10.1002/2016GL068180

Sanford, T. B. (1971). Motionally induced electric and magnetic fields in the sea. *Journal of Geophysical Research*, *76*(15), 3476–3492.

Saynisch, J., Petereit, J., Irrgang, C., & Thomas, M. (2017). Impact of oceanic warming on electromagnetic oceanic tidal signals: A CMIP5 climate model-based sensitivity study. *Geophysical Research Letters*, *44*, 4994–5000. https://doi.org/10.1002/2017GL073683

Schnepf, N., Kuvshinov, A., & Sabaka, T. (2015). Can we probe the conductivity of the lithosphere and upper mantle using satellite tidal magnetic signals? *Geophysical Research Letters*, *42*, 3233–3239. https://doi.org/10.1002/2015GL063540

Schnepf, N. R., Nair, M., Maute, A., Pedatella, N. M., Kuvshinov, A., & Richmond, A. D. (2018). A comparison of model-based ionospheric and ocean tidal magnetic signals with observatory data. *Geophysical Research Letters*, *45*, 7257–7267. https://doi.org/10.1029/2018GL078487

Thébault, E., Finlay, C. C., Beggan, C. D., Alken, P., Aubert, J., Barrois, O., et al. (2015). International geomagnetic reference field: The 12th generation. *Earth, Planets and Space*, *67*(1), 79.

Trossman, D., & Tyler, R. (2019). Predictability of ocean heat content from electrical conductance. *Journal of Geophysical Research: Oceans*, *124*, 667–679. https://doi.org/10.1029/2018JC014740

Tyler, R. H., Maus, S., & Lühr, H. (2003). Satellite observations of magnetic fields due to ocean tidal flow. *Science*, *299*(5604), 239–241.

Tyler, R. H., Mysak, L. A., & Oberhuber, J. M. (1997). Electromagnetic fields generated by a three dimensional global ocean circulation. *Journal of Geophysical Research*, *102*(C3), 5531–5551.

Velímsky, J., Grayver, A., Kuvshinov, A., & Šachl, L. (2018). On the modelling of M_2 tidal magnetic signatures: Effects of physical approximations and numerical resolution. *Earth, Planets and Space*, *70*(1), 192.